Article:

Culache, G., Byfield, M.P., Ferguson, N.S. et al. (1 more author) (2017) Robustness of beam-to-column end-plate moment connections with stainless steel bolts subjected to high rates of loading. Journal of Structural Engineering, 143 (6). 04017015. ISSN 0733-9445

https://doi.org/10.1061/(ASCE)ST.1943-541X.0001707

Robustness of beam to column end-plate moment connections with stainless steel bolts subjected to high rates of loading

G. Culache, M. P. Byfield, N. S. Ferguson, A. Tyas

Abstract

This paper presents an experimental investigation into end-plate beam column connections for buildings. The work demonstrates that a four-fold increase in the energy absorbed to failure can be achieved by replacing carbon steel bolts with their stainless steel counterparts. Experimental tests were carried out under load control and these provided the opportunity to observe the time required for connection fracture. Under quasi-static loading, connections tested with stainless steel bolts showed clearly visible signs of distress prior to failure; whereas the carbon-steel bolted equivalents provided no warning of failure prior to brittle fracture.

Experimental tests were carried out on bolts and these showed strain rate induced strength enhancements. End-plate connections were also tested under high strain rates. Loading rate was not observed to significantly affect the performance of stainless steel bolted connections. However, carbon-steel bolted connections were observed to weaken under high strain rates, therefore dynamically increased material properties did not always translate into increase connection strength. The design strengths predicted using Eurocode 3 were found to be in good agreement with the experimentally observed values under quasi-static loading for both bolt types. Under high-strain rate conditions the Eurocode 3 method was also found to provide a good prediction for stainless steel bolted connections; but was found to over predict for carbon-steel connections.

The simple modification of replacing carbon-steel bolts with their stainless steel equivalents is shown to be an effective way of improving the performance of industry standard connections. This modification is of relevance to the design of buildings and other structures in which the ductility is of high importance, for example in structures which may need to resist transient loads from blast or impact.

Introduction

During World War II a considerable amount of research was carried out into weapons effects on buildings by Lord John Baker and Sir Dermot Christopherson (Byfield 2006). Their forensic investigations identified a distinct weakness in the beam-column connections used during that time in multi-storey steel framed buildings. They concluded that the majority of collapses caused by bombs could be traced back to connection failures (Byfield 2006; Smith et al. 2010) and one of their main recommendations was that full-moment joints should be provided when blast resistance is required (Smith et al. 2010).

The need for the adequate tying of load bearing members was highlighted by the partial collapse of the Ronan Point apartment building in 1968, after which regulations were introduced in the United Kingdom defining the tying forces that beam connections must be able to resist without fracture. The objective was two-fold: to help keep members tied together when subjected to lateral loads; and to enable columns to be supported by catenary action in the event of column damage. The importance of providing adequate tying was well known to World War II investigators, who often observed beam-column connection failures occurred due to the suction pressures which develop when bombs detonate near buildings (near misses) (Byfield 2006; Smith et al. 2010). The tie force regulation did not however stipulate rotation requirements and it was subsequently demonstrated that the industry standard connections used in most United Kingdom steel framed buildings lack the rotation capacity to support columns through catenary action (Byfield & Paramasivam 2007). Despite this short-coming, the tie force method remains popular with regulators and has been incorporated into Eurocode 1 (CEN 2005a).

The collapse of the World Trade Centre buildings in New York in 2001 led to a renewed interest into improving the robustness of buildings. The aircrafts penetrated far enough that they adversely affected the emergency exits blocking occupants in the upper stories of the towers and initiating the collapse of the structures (Federal Emergency Management Agency 2002; National Commission on Terrorist Attacks 2004). These events and others in the past two decades led to reports summarising that one of the key safety issues in tall buildings is vulnerability to progressive collapse and the following major conclusion was consistently reiterated (Shyam-Sunder 2005; Federal Emergency

Management Agency 2002): *"This vulnerability is directly related to the strength, ductility and hence* the energy absorption capacity of *the connections between the main structural elements."* (Institution of Structural Engineers 2002)

These events also led to an intensification of research activity on progressive collapse with an increase in publications from 20 papers between 1992 and 2000 to over 450 papers between 2002 and 2012 (El-Tawil, S., Li, H., Kunnath 2014). As there is significant risk, cost and effort associated with high-quality experimental testing and the fact that it is often carried out by organizations that restrict publication of data, computational modelling and simulation represent the primary tools in this research area.

Whole frame numerical models which incorporate perfectly pinned or perfectly-rigid connections have been shown to be inadequate when modelling progressive collapse (Stoddart 2012) or blast structure interaction (Stoddart et al. 2013). Equally, using full three-dimensional connection models with non-linear material models may create computational overload when used for modelling whole frames dynamically. Representing connections as non-linear springs has also been shown to present problems, because the horizontal forces which develop affect the joint stiffness, which cannot be accounted for with a single non-linear spring element (Stoddart et al. 2013). This problem also occurs during the modelling of frames subjected to fire, where thermal expansion, followed by catenary action at higher temperatures induces high horizontal forces. This problem was overcome by Yu et al. (Yu et al. 2009a; Yu et al. 2009b) who incorporated temperature dependent component models into whole frame models. This avoids computational overload and was shown to accurately model experimentally observed behaviour. This technique was subsequently shown to work for modelling progressive collapse and blast structure interaction modelling (Stoddart 2012), (Stoddart et al. 2013), but using strain rate dependent material models based on the Malvar and Crawford constitutive model (Malvar 1998).

As specialist high-strain rate tests are costly, many investigations have relied upon computational modelling in the absence of experimental work. The importance of physical tests was recognised by El-Tawil et al. (El-Tawil, S., Li, H., Kunnath 2014) who stated that "One of the greatest needs at the moment is for high-quality test data at the component and subassembly levels. These tests will provide the necessary data for validation of modelling tools and development of design guidelines" (El-Tawil, S., Li, H., Kunnath 2014).

The National Institute of Standards and Technology conducted a series of full-scale tests supported by advanced numerical modelling of beam-column assemblies (Sadek et al. 2011). These simulated column removal scenarios, with each assembly consisting of three columns and two beams. Each was subject to vertical displacement of the centre column until failure under quasi-static loading rates (Lew et al. 2013). The novelty was in the creation of an improved connection with a reduced beam section in its proximity. This improved ductility, increased ultimate deflections and loads. Reduced finite element models, where three dimensional components were replaced with an assembly of simplified two dimensional elements and rigid links, achieved a high degree of accuracy without computational overload (Sadek et al. 2013).

Izzuddin and Vlassis (Vlassis et al. 2008; Izzuddin et al. 2008) also mention the need for further development in simplified modelling of connections and for the realistic representation of the nonlinear response of various connection types under dynamic loading conditions. Structures subjected to blast and to a lesser extent progressive collapse, are subjected to high strain rates, and these are known to affect both the strength and ductility of the materials. For this reason high strain rate tests are particularly useful when investigating the performance of structures subjected to blast. It is generally accepted that in the case of pure tensile testing of steel coupons and bars that the yield and ultimate stresses increase with very high strain rates (Malvar 1998; Meyers 1994). This increase can influence connection behaviour and it can be modelled using the dynamic increase factor (DIF) for stress . Christopherson (Christopherson 1945) warned against the general application of a dynamic increase factor for steel material properties during design, because he found that dynamic properties lack reliability (Smith et al. 2010).

Models for the dynamic increase factor (DIF) of yield stress with strain rate are available (Malvar 1998), (Johnson & Cook 1983). However, the increase in strength with high strain rates is not necessarily applicable to bolts tested under high strain rates, due to the fact that bolts may fail through a variety of failure mechanisms such as thread stripping (Mouritz 1994). Mouritz was one of the first to conduct investigations into the behaviour of bolt-nut assemblies under strain rates that varied from 10^{-}

^{5} s^{-1} in tensile testing to 10^{3} s^{-1}. He concluded that as the strain rate increases the threads are increasingly likely to fail at lower fractions of the shank strength. Research carried out by Munoz-Garcia et al. showed that M20 grade 8.8 fail through thread stripping and that the strength decreased with increasing strain rates (Munoz-Garcia et al. 2005). Their experimental study included strain rates up to 20 s^{-1}. Munoz-Garcia et al. (2005) found that M12 grade A4-70 stainless steel bolts fail at the much larger failure strain of 16% as opposed to the 2-3% strain at which black carbon steel bolts fail.

Tyas et al. (2012) developed a testing rig for the combined rotation-extension testing of nominally-pinned steel beam to column joints at high rates of loading. Loading time scales varied between a few milliseconds and several minutes. Results showed that simple flexible end plate connections show a decrease in ductility when failed at high strain rates.

Experimental tests were carried out at the University of Coimbra on T-stub components subjected to impact loading (Barata et al. 2014) and numerical models were created that accurately captured behaviour at both low and high strain rates (Ribeiro, Santiago, Rigueiro, et al. 2015), (Ribeiro et al. 2016). Experimental tests and numerical modelling were also carried out on moment connections at low and high strain rates. The experiments show that the dynamic increase factor of the steel is reflected on the resistance of the connection as a whole, giving the connection a higher moment capacity (Ribeiro, Santiago & Rigueiro 2015). Experimental tests simulating a column removal scenario under both low and high strain rates, 10^{-3} s^{-1} to 10^{2} s^{-1}, were carried out at the Norwegian University of Science and Technology (Grimsmo et al. 2015). These showed that a more symmetrical deformation mode was obtained in the dynamic case leading therefore to an increase in the energy absorbed by the connection in the dynamic case. In both cases, the aforementioned investigations always used two nuts on grade 8.8 bolts in order to avoid thread stripping as a bolt failure mechanism.

Experimental work in the area of moment connections so far focused on testing connection with 2 or 3 bolt rows (Simões da Silva et al. 2001; Simões da Silva et al. 2002; Ribeiro, Santiago, Rigueiro, et al. 2015; Kuhlmann et al. 2009; Grimsmo et al. 2015), see Fig. 1 (a). However, industry standard connections of high moment capacity often consist of end plates with five or more bolt rows (SCI/BCSA Connections Group 1995), see Fig. 1 (b). Thus the tests carried out in this investigation included 5 and 7 bolt rows in order to investigate the performance of connections with more than 3 bolt rows.

Experimental programme

This experimental test programme was designed to investigate the moment vs. rotation response of end-plate connections under quasi-static loading, as well as high strain rate loading. This could be from the demands imposed by the catenary action which follows sudden column removal in a building or the higher rates of loading developed from blast waves. The load was maintained throughout all of the tests in order to investigate the time to fracture.

Connections tested and design methodology

This investigation explored the behaviour of extended end-plate and flush end-plate beam to column connections. Fig. 2 shows the dimensions of the connections tested. Each connection was tested with either M12 grade 8.8 carbon steel bolts or M12 grade A4-70 stainless steel bolts. All end plates were 12mm thick. All bolts were tested with one nut only.

Every connection was tested both statically and dynamically leading to eight different testing configurations. The details of each test are listed in Table 1. Loading times and loading rates were recorded during the tests and used to estimate the strain rates involved in the testing, see Table 1.

The moment connections were designed in accordance with Eurocode 3 (CEN 2005b) using the methodology presented in industry design guides (SCI/BCSA Connections Group 2013) and (CEN 2005b). The connections were dimensioned in order to obtain failure of the connection by either bolt failure, yielding of the end plate, buckling of the bottom flange of the beam stub, or a combination of these modes. The resistance of a bolt row is given by the resistance of the equivalent T-stub. The T-stub can fail in three different modes as shown in Fig. 3:

- In mode 1 through complete flange yielding
- In mode 2 through bolt failure with flange yielding
- In mode 3 through bolt failure

The compression resistance of the combined beam flange and web in the compression zone is $F_{c,fb,Rd}$. Expressions for calculating the tensile forces in the T-stubs $F_{T,1-3,Rd}$ and $F_{c,fb,Rd}$ are provided in the Eurocode (CEN 2005b). The predicted values for the tested connections together with the assumed distributions are presented in Fig. 4. The design moment resistance of the connection ($M_{j,Rd}$) is given by:

$$M_{j,Rd} = \sum_r h_r F_{tr,Rd} \quad (1)$$

where $F_{tr,Rd}$ is the effective design tension resistance of bolt row r, h_r is the distance from bolt row r to the centre of the compression and r is the bolt row number.

The Eurocode (CEN 2005b) defines a partial-strength joint as one which has a design moment resistance lower than the plastic moment of resistance of the connected beam or column. In all cases the calculated moment capacity of the connections was less than the capacity of the beam. The extended end-plate connection achieves 77-78% of the beam capacity, whereas the flush-end-plate only 47-48%, see Table 2. Consequently all connection types are classified as partial strength according to the Eurocode (CEN 2005b).

Material properties

Tensile tests on the bolts and steel coupons taken from the end plate steel were carried out at strain rates $\dot{\varepsilon}$ ranging from 0.001/s to 1/s, see Table 3. A purpose-built testing rig was designed for testing the bolts in tension so that they have the same engaged length as in the connection tests and that would allow these to be tested within the aforementioned range of strain rates. Force versus displacement curves for carbon steel and stainless steel bolt tests are shown in Fig. 5 for selected strain rates. The bolts had an engaged length, between the bolt head and the nut, of approximately 35mm and only one nut was used. This engaged length corresponded with that used in the actual joint tests.

As long as one nut was used, carbon steel bolts were always observed to fail through thread stripping; see Fig. 6. The force-displacement curves for black bolts show a steep rise followed immediately by a steep decline. After the nut thread was stripped, the nut slid over the rest of the thread of the bolt, providing very little resistance in the process. The average energy absorbed by a carbon-steel bolt is 0.48 kJ and the nut travels for less than 4mm in the static case before thread stripping commences and the resistance decreases sharply.

The stainless steel bolts were always observed to fail through necking of the bolt shank and ductile fracture of the neck; see Fig. 6. As a consequence the bolts absorb more energy, with the average being

1.13 kJ. The elongation in the static case was observed to be up to 16mm, providing more ductility than the carbon steel bolts. This failure mode is counter-intuitive since the tensile area in the threaded region is smaller than the tensile area of the bolt body. This behaviour is explained by the local increase in the strength levels for austenitic grades by cold working of the thread during manufacture (SCI/EuroInox 2006). This reference (SCI/EuroInox 2006) reported that the 0.2% proof strength is typically enhanced by a factor of 50% in the corners of the thread by cold forming. It is possible that shank failure was obtained due to the high local strength of the threaded region of austenitic stainless steel. The failure mechanisms and the differences in ductility are consistent with research carried out by Munoz-Garcia et al. (Munoz-Garcia et al. 2005). Thread stripping as a failure mechanism for carbon steel bolts was also observed in tests at the University of Coimbra, Barata et al. (Barata et al. 2014), and at the Norwegian University of Science and Technology, Grimsmo et al. (Grimsmo et al. 2015).

It was observed that the strength of both bolt types increases with increasing strain rates.

The Johnson-Cook (1983) model defines the relationship between stress and strain rates:

$$\sigma = (\sigma_0 + K\varepsilon^n)\left(1 + C_0\, ln\frac{\dot{\varepsilon}}{\dot{\varepsilon}_0}\right)\left[1 - \left(\frac{T - T_r}{T_m - T_r}\right)^m\right] \tag{2}$$

where σ is the stress, σ_0 is the yield stress under static conditions, the constants K, n and m are material parameters, T_r is the reference temperature, T_m the melting point, $\dot{\varepsilon}_0$ the reference strain rate, and importantly here the C_0 parameter characterises the strain-rate dependence of stress.

Assuming a similar relationship is true for the ultimate bolt force, this model was used in a simplified form to inform on the C parameter and quantify the dynamic increase in the bolt force with strain rate. Considering only strain rate dependence, the DIF was expressed as:

$$DIF_{bolt} = \frac{F_{dynamic}}{F_{static}} = 1 + C\, ln\frac{\dot{\varepsilon}}{\dot{\varepsilon}_0} \tag{3}$$

where the C parameter characterises the strain-rate dependence of force.

The dynamic increase factor for ultimate force is plotted for corresponding strain rates in Fig. 7 for both bolt types. Logarithmic trend lines and their equations are shown on the graph together with the equivalent Johnson-Cook C parameters. The C parameters are 0.0047 and 0.0069 for carbon steel and stainless steel respectively.

With increasing strain rates, a decrease in ductility was observed in both bolt types. In the case of the stainless steel bolts the fracture strain can be estimated using measurements of the initial radius and the radius of the neck at fracture (Bao & Wierzbicki 2004). The relationship between the fracture strain ratio and strain rate is shown in Fig. 8. The fracture strain reduces with increased strain rate.

Tensile tests were also carried out for steel coupons cut from the beam stubs and end plates for the same range of strain rates. The stress-strain relationship for the S355 end plate steel is shown in Fig. 9 for two selected strain rates. In the case of the S355 steel it was observed that the dynamic effect is greater on the yield stress than on the ultimate stress, which is consistent with Malvar and Crawford (Malvar 1998).

Connection test rig set-up

Most tests of this kind are carried out under controlled displacement, allowing the load to reduce slowly and failure to occur in a safe manner. In this investigation the load was maintained during failure and arguably this more closely matches the loading experienced in a real structure.

A 3D diagram of the testing rig used to carry out the experimental tests is shown in Fig. 10. In the quasi-static tests the pressure is released through a cylinder and slowly increased to push the piston or loading ram. Load is applied through the loading ram at one end of the “flying column” and was measured using a load cell; see Fig. 10. The term “flying” is used because the column is supported by roller bearings and is free to slide freely as soon as the connection fractures. The loading rates, approximate strain rates and video frames per second are shown in Table 1

Displacements were measured at five points using laser displacement gauges (LDGs), shown schematically in Fig. 11. LDG1 and LDG2 measured the displacement of the “flying column” in the direction of the loading ram. These measurements enabled calculation of the rotation α of the column. LDG3 measured the axial displacement of the “column”. LDG4 and LDG5 were located to measure displacements of the angles and these were used to calculate the rotation β of the angles.

From force and moment equilibrium, Fig. 12 (a), the connection force and moment are given by:

$$F_C = F_A \tag{4}$$

$$M_C = d \cdot F_A \tag{5}$$

where F_C and M_C are the connection force and moment, F_A is the load applied, and d is the distance between the loading ram and the centre of the moment connection. Distance d is equal to $1105mm$ in all tests. Fig. 12 (b) presents the load applied F_A versus time for test T2A to exemplify the general character of loading in quasi-static cases.

In the case of dynamic loading of the connection, inertia effects are no longer negligible. From force and moment equilibrium, Fig. 13 (a), the connection force is given by:

$$F_C(t) = F_A(t) \cdot cos[\theta(t)] - F_I(t) = F_A(t) \cdot cos[\theta(t)] - m_c\ddot{\delta}_c \tag{6}$$

where F_C is the connection force, F_A is the applied load, F_I is the inertia force, m_c is the mass of the flying column and extension piece and $\ddot{\delta}_c$ is acceleration of the centre of mass. Fig. 13 (b) presents the load applied F_A versus time for test T4 to exemplify of the general character of loading in dynamic cases.

In order to calculate the connection moment the equilibrium equation for moments is written so that inertia effects are taken into account resulting in the following equation:

$$M_C(t) = d_{cm1} \cdot F_A(t) \cdot cos[\theta(t)] + d_{cm2} \cdot F_C(t) - I_{mc} \cdot \ddot{\theta}(t) \tag{7}$$

where M_C is the connection moment, d is the distance between the loading ram and the centre of the connection, d_{cm1} is the distance between the loading ram and centre of mass, d_{cm2} is the distance between the centre of mass and the centre of the connection, I_{mc} is the mass moment of inertia about the centre of mass and was calculated as 339kgm^2. It was observed in the experiments that both the column and the angle supports rotated; see Fig. 11 (b). This was considered and displacements were recorded at the ends of both. The rotations of the column α and angles β, and the relative rotation θ are given by:

$$\alpha = \tan^{-1}\left(\frac{\delta_1 - \delta_2}{d_{12}}\right) \tag{8}$$

$$\beta = \tan^{-1}\left(\frac{\delta_4 - \delta_5}{d_{45}}\right) \tag{9}$$

$$\theta = \alpha - \beta \tag{10}$$

where δ_1 and δ_2 are the displacements at the ends of the column, d_{12} is the distance between the two laser gauges pointed at the column, δ_4 and δ_5 are the displacements at the ends of the angles, and d_{45}

is the distance between the two laser gauges pointed at the angles. Fig. 14 shows the rotation of the "flying column" α and of the supporting angles β in dynamic test T4. All subsequent graphs are plotted versus the relative rotation θ.

Results

The strength, ductility and energy absorbed for each connection test is summarised in Table 4. The design moment capacities do not include factors of safety, which were removed in order to more clearly reveal the accuracy of the Eurocode 3 design expressions. There was a good agreement between the predicted and experimental test results under quasi-static loading. Under dynamic loading the stainless steel flush end-plate connection strengthened, as would be expected from the dynamic increase in material properties discussed earlier. The stainless steel extended end-plate connection weakened under dynamic loading, but still achieved the design strength. This connection failed by flange buckling and this may have prevented a dynamic strength increase developing, although this is discussed in more detail later. The experimental testing of carbon-steel bolts under high strain rates would suggest an increase in strength of the connections under high strain-rate loading, although this was not observed. In fact these connections were significantly understrength and this highlights the known reliability problems when using dynamic increase factors for material properties for calculating design strengths (Smith et al. 2010). Important from a robustness point of view, stainless steel bolted connections can be seen to have absorbed approximately 4 times the energy of the carbon steel connections.

Quasi-static connection tests

Fig. 15 shows the moment rotation behaviour for the static tests with values of strength labelled at selected points. The tests loaded the connections over a period of approximately 300 seconds, after which failure occurred in less than 100 milliseconds. The carbon steel bolts reached their ultimate strength with no significant plastic deformation of the end plate, after which they failed in a brittle manner. This is evident both in the moment versus rotation relationships, where the maximum rotation is found to be just over 1 degree, as well as from the photographs of the connections taken after failure.

The stainless steel bolts deformed plastically and this caused significantly more deformation in the plate than for the carbon steel bolted connections, see Fig. 16. It is important to note that bottom flange buckling was observed in the case of the extended end-plate connection with stainless bolts. The compression flange buckles and plastic deformation spreads through the web in compression. Referring to the possible failure modes of a T-stub in Fig. 3, the carbon steel bolts led to a mode 3 failure. Although the stainless steel bolts have a lower ultimate strength than carbon steel bolts, they changed the T-stub to a mode 2 failure due to their superior ductility. Thus, the ductility of stainless bolts is reflected in an increase in the ductility of the connections.

Dynamic connection tests

When the connections were loaded dynamically the moment increases to a first initial peak value in a time period of 4 milliseconds. In test T7, after the first peak, the resistance of the carbon steel bolted connection plateaus for 6 milliseconds as the threads of the nut deform plastically, Fig. 17. Once the deformation commenced the resistance of the connection decreased linearly to zero in less than 20ms. As the high-speed digital camera frame rate was 500fps, the entire loading and failure was captured with sufficient detail to understand the failure process. Fig. 17 shows three frames at the commencement of thread stripping, during the process, and after most threads are completely stripped. The end plate remains flat during this process.

In test T4 (the stainless steel bolted connection shown in Fig. 17) the extended end plate and bolts are seen to deform plastically, resulting in a gradual increase in moment capacity. The frame captured at 22ms shows significant plastic deformation of the end plate, the bolts, and the asymmetrical buckling of the compression flange. Moment versus rotation relationships are presented in Fig. 18 for the extended end plate connection together with the static loading cases. This asymmetric buckling may be the cause of the reduction in the dynamic strength of the extended end-plate connection. In comparison, flange buckling did not occur in the flush end-plate connection. The absence of this failure mode may have allowed the stainless steel flush end-plate connection to develop a dynamic strength increase, as was expected from the bolt material property tests.

A similar sequence of events was observed for the dynamic tests of the flush end plate connections. Several important differences must be noted in test T11 on the stainless steel bolted flush connection,

Fig. 19. Here there was no buckling of the bottom flange and this is the only test where a dynamic increase in the moment capacity of the whole connection was observed, as Fig. 19 illustrates.

In the carbon steel bolted connections thread stripping leads to a rapid loss of connection strength. In the case of the stainless steel bolted end-plate connections, the bolt ductility provides time for end-plate deformation before final failure, allowing for greater overall connection ductility, as illustrated by the difference between top row and bottom row of images in Fig. 17.

Conclusions

Experimental tests on bolts have been presented. These were carried out under quasi-static and elevated strain rates. Carbon steel bolts are shown to fail through thread stripping, whereas ductile necking was observed in stainless steel bolts. Both bolt types showed strength enhancement under elevated strain rates, in a manner consistent with the literature. However, these strength enhancements did not always translate into increased connection strength. The stainless steel bolted connections were found to absorb the same amount of energy before failure under static and high strain-rate loading. They were also shown to be able to achieve their design values of strength under high-strain rate loading. In comparison, the carbon steel connections were found to be under-strength under high strain-rate loading; i.e. the dynamic increase in material properties demonstrated in the bolt tests did not translate into increased connection strength under high-strain rate loading.

The quasi-static experimental connection strengths showed good agreement with the Eurocode 3 design strengths for carbon steel and stainless steel connections. During the quasi-static tests loading occurred over a time period of 300 seconds, after which failure occurred in an explosive manner in less than a 1/10th of a second. The carbon steel bolted connections reached their ultimate strengths with no observable plastic deformation, whereas failure was preceded by extensive plastic deformation in both the bolts and the end-plates in the stainless steel bolted connections.

This research demonstrates that the simple replacement of carbon-steel bolts with their stainless steel equivalent will improve strength, ductility and the ability to resist dynamic loading for the end-plate beam-column connections investigated.

Acknowledgements

The investigators would like to thank the Defence Science and Technology Laboratory, part of the Ministry of Defence (United Kingdom) for funding this research.

References

Bao, Y. & Wierzbicki, T., 2004. On fracture locus in the equivalent strain and stress triaxiality space. International Journal of Mechanical Sciences, 46(1), pp.81–98.

Barata, P. et al., 2014. Experimental analysis of a T-stub component subjected to impact loading. Naples: EUROSTEEL.

Byfield, M.P., 2006. Behavior and Design of Commercial Multistory Buildings Subjected to Blast. Journal of Performance of Constructed Facilities, 20(4), pp.324–329.

Byfield, M.P. & Paramasivam, S., 2007. Catenary action in steel-framed buildings. Structures and Buildings, 160(5), pp.247–257.

CEN, 2005a. BS EN 1991-1-7:2006+A1:2014 Eurocode 1. Actions on structures. General actions. Accidental actions, European Committee for Standardization (CEN).

CEN, 2005b. BS EN 1993-1-8:2005 Eurocode 3: Design of steel structures - Part 1-8: Design of Joints.

Christopherson, D.G., 1945. Structural defence, London.

El-Tawil, S., Li, H., Kunnath, S., 2014. Computational Simulation of Gravity-Induced Progressive Collapse of Steel-Frame Buildings: Current Trends and Future Research Needs. J. Struct. Eng., 140(SPECIAL ISSUE: Computational Simulation in Structural Engineering). Available at: http://ascelibrary.org/doi/abs/10.1061/%28ASCE%29ST.1943-541X.0000897.

Federal Emergency Management Agency, 2002. World Trade Center Building Performance Study. FEMA 403., Washington, DC.

Grimsmo, E.L. et al., 2015. An experimental study of static and dynamic behaviour of bolted end-plate joints of steel. International Journal of Impact Engineering, 85, pp.132–145. Available at:

http://www.sciencedirect.com/science/article/pii/S0734743X15001554 [Accessed October 15, 2015].

Institution of Structural Engineers, 2002. Safety in tall buildings and other buildings with large occupancy,

Izzuddin, B.A. et al., 2008. Progressive collapse of multi-storey buildings due to sudden column loss — Part I: Simplified assessment framework. Engineering Structures, 30(5), pp.1308–1318. Available at: http://www.sciencedirect.com/science/article/pii/S0141029607002805.

Johnson, G.R. & Cook, W.H., 1983. A constitutive model and data for metals subjected to large strains, high strain rates and high temperatures. Proc. 7th int. symp. on ballistics, p.7.

Kuhlmann, U. et al., 2009. Robust structures by joint ductility, Brussels.

Lew, H.S. et al., 2013. Performance of Steel Moment Connections under a Column Removal Scenario. I: Experiments. J. Struct. Eng., 139(1), pp.98–107.

Malvar, L.J., 1998. Review of Static and Dynamic Properties of Steel Reinforcing Bars. Materials Journal, 95(5), pp.609–616.

Meyers, M.A., 1994. Dynamic Behaviour of Materials 1st ed., Wiley-Interscience.

Mouritz, A.P., 1994. Failure mechanisms of mild steel bolts under different tensile loading rates. Int J Impact Eng, 15(3), p.14.

Munoz-Garcia, E., Davison, J.B. & Tyas, A., 2005. Analysis of the response of structural bolts subjected to rapid rates of loading. 4th European Conference on Steel and Composite Structures, Eurosteel 2005, C(4.10), pp.147–154.

National Commission on Terrorist Attacks, 2004. The 9/11 Commission Report,

Ribeiro, J., Santiago, A., Rigueiro, C., et al., 2015. Analytical model for the response of T-stub joint component under impact loading. Journal of Constructional Steel Research, 106, pp.23–34. Available at: http://www.sciencedirect.com/science/article/pii/S0143974X14003241 [Accessed March 15, 2015].

Ribeiro, J. et al., 2016. Numerical assessment of T-stub component subjected to impact loading. Engineering Structures, 106, pp.450–460. Available at: http://www.sciencedirect.com/science/article/pii/S0141029615006811 [Accessed November 20, 2015].

Ribeiro, J., Santiago, A. & Rigueiro, C., 2015. Numerical assessment of beam-to-column steel joints subjected to impact loading. In Eigth International Conference on Advances in Steel Structures.

Sadek, F. et al., 2013. Performance of Steel Moment Connections under a Column Removal Scenario. II: Analysis. J. Struct. Eng., 139(1), pp.108–119.

Sadek, F. et al., 2011. Testing and Analysis of Steel and Concrete Beam-Column Assemblies under a Column Removal Scenario. J. Struct. Eng., 137(SPECIAL ISSUE: Commemorating 10 Years of Research since 9/11), pp.881–892.

SCI/BCSA Connections Group, 1995. Joints in steel construction: Moment Connections, The British Constructional Steelwork Association/The Steel Construction Institute.

SCI/BCSA Connections Group, 2013. Joints in steel construction: Moment-resisting joints to Eurocode 3 (P398), The Steel Construction Institute and The British Constructional Steelwork Association.

SCI/EuroInox, 2006. Design manual for structural stainless steel 3rd ed., Euro Inox and The Steel Construction Institute.

Shyam-Sunder, S., 2005. Federal Building and Fire Safety Investigation of the World Trade Center Disaster: Final Report of the National Construction Safety Team on the Collapses of the World Trade Center Towers (NIST NCSTAR 1),

Simões da Silva, L., Santiago, A. & Vila Real, P., 2002. Post-limit stiffness and ductility of end-plate beam-to-column steel joints. Computers & Structures, 80(5-6), pp.515–531. Available at: http://www.sciencedirect.com/science/article/pii/S0045794902000147 [Accessed October 15, 2015].

Simões da Silva, L., Simões, R.D. & Cruz, P.J.S., 2001. Experimental behaviour of end-plate beam-to-column composite joints under monotonical loading. Engineering Structures, 23(11), pp.1383–1409. Available at: http://www.sciencedirect.com/science/article/pii/S0141029601000542 [Accessed May 6, 2015].

Smith, P., Byfield, M.P. & Goode, D., 2010. Building Robustness Research during World War II. J. Perform. Constr. Facil., 24(6), pp.529–535.

Stoddart, E.P., 2012. Development of Component-based Connection Modelling for Steel Framed Structures Subjected to Blast or Progressive Collapse. Southampton: University of Southampton.

Stoddart, E.P. et al., 2013. Strain rate dependent component based connection modelling for use in non-linear dynamic progressive collapse analysis. Engineering Structures, 55(0), pp.35–43. Available at: http://www.sciencedirect.com/science/article/pii/S0141029612002854.

Tyas, A. et al., 2012. A Methodology for Combined Rotation-Extension Testing of Simple Steel Beam to Column Joints at High Rates of Loading. Experimental Mechanics, 52(8), pp.1097–1109.

Vlassis, A.G. et al., 2008. Progressive collapse of multi-storey buildings due to sudden column loss—Part II: Application. Engineering Structures, 30(5), pp.1424–1438. Available at: http://www.sciencedirect.com/science/article/pii/S0141029607003239.

Yu, H. et al., 2009a. Development of a yield-line model for endplate connections in fire. Journal of Constructional Steel Research, 65(6), pp.1279–1289. Available at: http://www.sciencedirect.com/science/article/pii/S0143974X08002824 [Accessed March 15, 2015].

Yu, H. et al., 2009b. Tying capacity of web cleat connections in fire, Part 2: Development of component-based model. Engineering Structures, 31(3), pp.697–708. Available at: http://www.sciencedirect.com/science/article/pii/S0141029608003659 [Accessed October 26, 2015].

Test No.	End plate type	Section size	Bolts type	Loading	Loading time	Loading rate	Approx. strain rates in the bolts	Video frames per second
T1	Extended	305x102x25	CS	Static	300 s	0.40 kN/s	0.002/s	10
T2A	Extended	305x102x25	SS	Static	300 s	0.40 kN/s	0.002/s	500
T7	Extended	305x102x25	CS	Dynamic	40 ms	20 kN/ms	20/s	500
T4	Extended	305x102x25	SS	Dynamic	40 ms	20 kN/ms	20/s	8000
T5	Flush	305x127x37	CS	Static	300 s	0.40 kN/s	0.002/s	500
T6	Flush	305x127x37	SS	Static	300 s	0.40 kN/s	0.002/s	500
T8	Flush	305x127x37	CS	Dynamic	40 ms	20 kN/ms	20/s	500
T11	Flush	305x127x37	SS	Dynamic	40 ms	20 kN/ms	20/s	8000

Table 1: Experimental test programme (Note: CS denotes Carbon Steel, SS denotes Stainless Steel)

Plate type	Bolts type	Connection design moment capacity with safety factors $M_{j,Rd}$ (kNm)	Connection design moment capacity without safety factors $M^{*}{}_{j,Rd}$ (kNm)	Beam stub capacity $M_{c,Rd}$ (kNm)	Percentage of beam capacity
Extended	CS	84	117	150 kNm	78%
Extended	SS	83	115	150 kNm	77%
Flush	CS	76	105	215 kNm	48%
Flush	SS	73	101	215 kNm	47%

Table 2: Design moment capacities of tested connection types

Connection element	Material designation	Average yield stress, f_y (N/mm^2)	Average ultimate tensile stress, f_u (N/mm^2)
305x102x25 UKB	S355	440 N/mm^2	530 N/mm^2
305x127x37 UKB	S355	400 N/mm^2	520 N/mm^2
End plate, 12mm thick	S355	407 N/mm^2	560 N/mm^2
M12 carbon steel bolts	Grade 8.8	-	935
M12 stainless steel bolts	A4-70	-	891

Table 3: Measured quasi-static material properties

Test	Connection type	Bolt type	Loading type	Design capacity* M_{Rd} (kNm)	Experimental capacity M_{RExp} (kNm)	Rotation capacity φ_{exp} $(°)$	Absorbed energy E (kJ)
T1	Extended	Carbon steel	Static	117	127	1.20	2.0
T2A	Extended	Stainless steel	Static	115	133	4.22	8.3
T7	Extended	Carbon steel	Dynamic	117	90	0.70	2.5
T4	Extended	Stainless steel	Dynamic	115	115	4.40	8.3
T5	Flush	Carbon steel	Static	105	98	1.20	1.6
T6	Flush	Stainless steel	Static	101	105	3.42	6.9
T8	Flush	Carbon steel	Dynamic	105	87	0.80	1.8
T11	Flush	Stainless steel	Dynamic	101	115	3.50	6.9

Table 4: Connection test results (* calculated without safety factors)

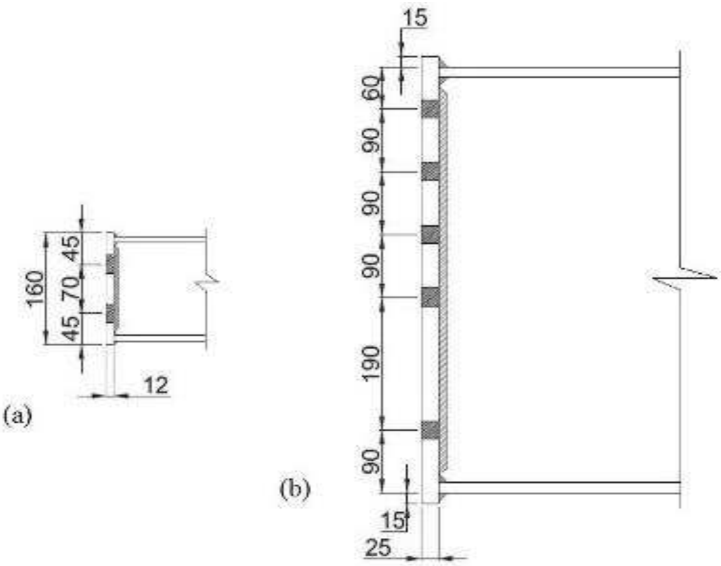

Fig. 1: (a) Connection tested at University of Liege (Kuhlmann et al. 2009) and (b) example of an industry-standard 5 bolt row connection (SCI, 1995)

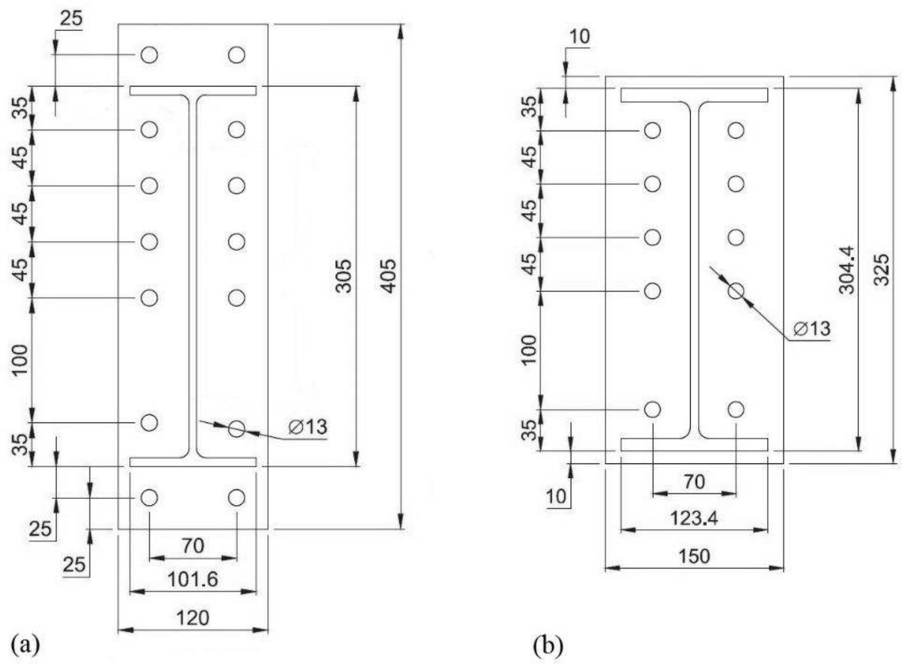

Fig. 2: Dimensions of (a) extended end-plate connection and (b) flush end-plate connection

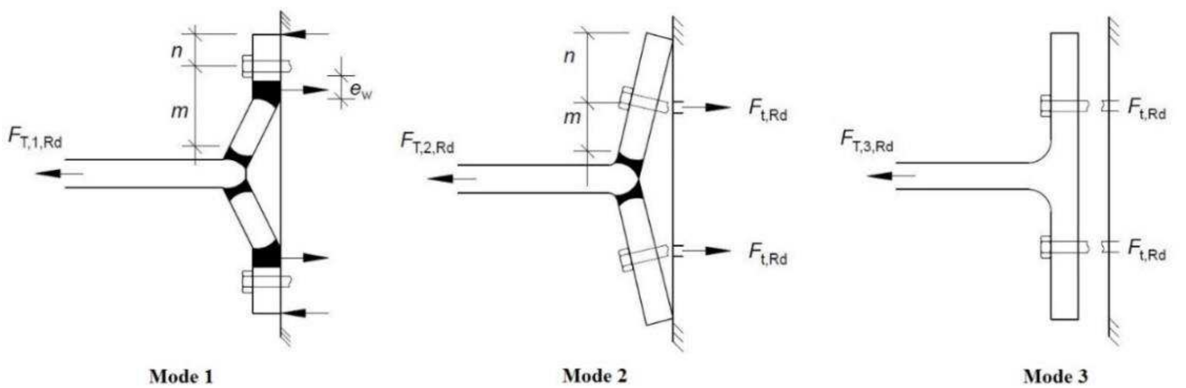

Fig. 3: Possible failure modes of the T-stub (SCI, 2013)

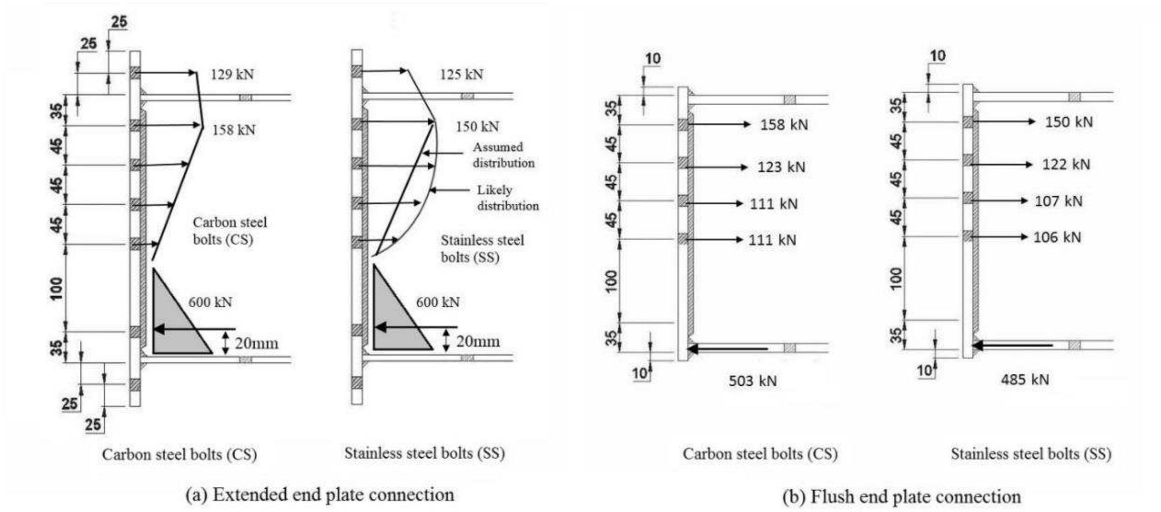

Fig. 4: Force distributions for the calculated design moment capacities

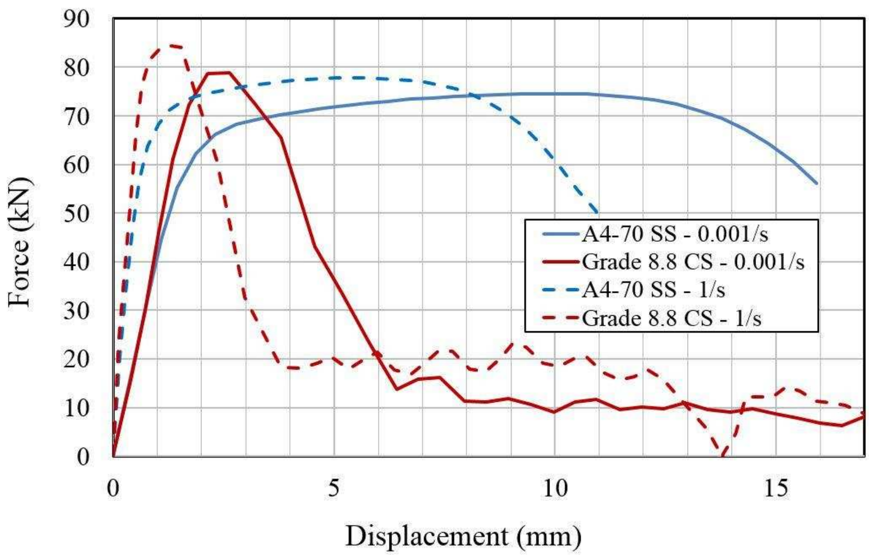

Fig. 5: Tensile tests of carbon steel (CS) and stainless steel (SS) bolts at selected strain rates

Fig. 6: Photos of failed bolts showing failure mechanism

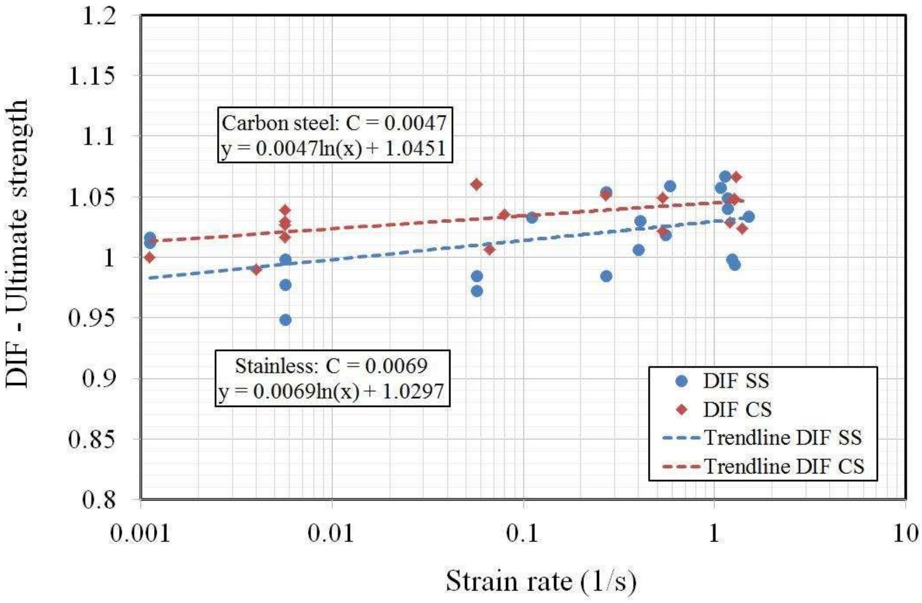

Fig. 7: Dynamic increase factor (DIF) versus strain rate from bolt tests

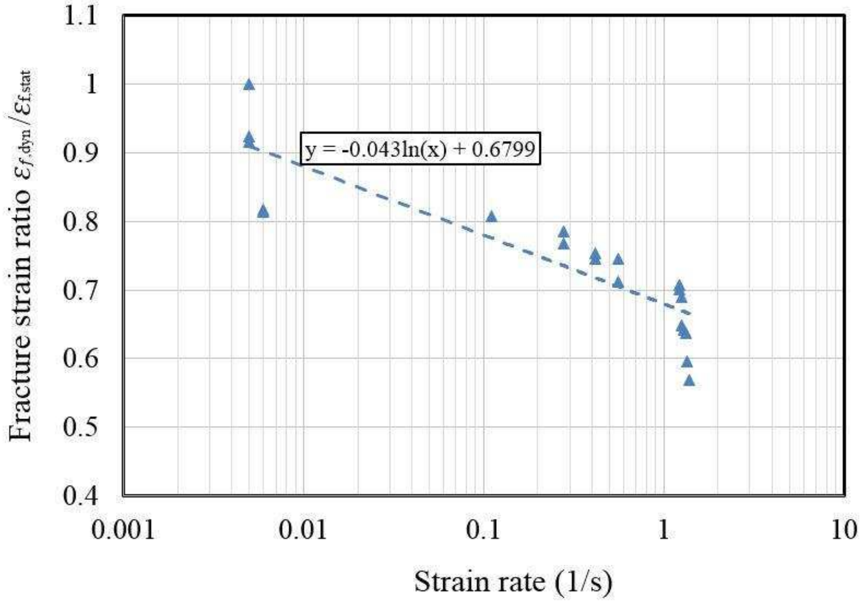

Fig. 8: Fracture strain ratio versus strain rate for stainless steel bolts

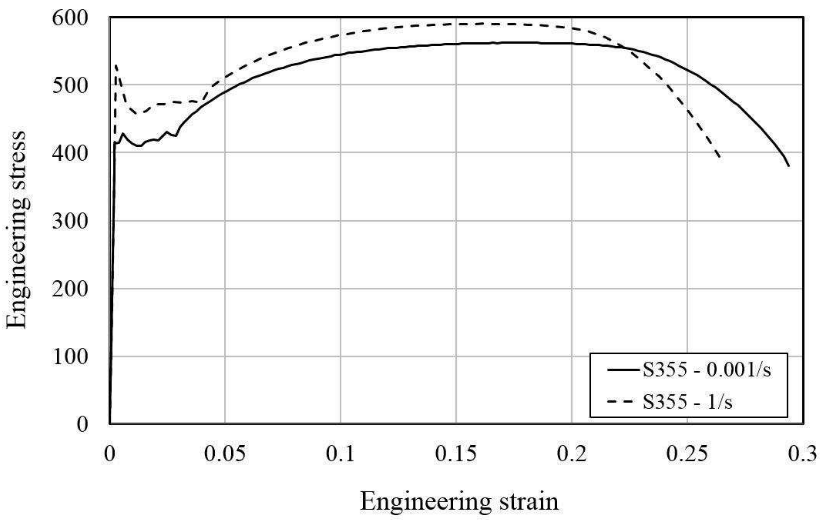

Fig. 9: Engineering stress strain curves for S355 steel taken from end plate for selected strain rates

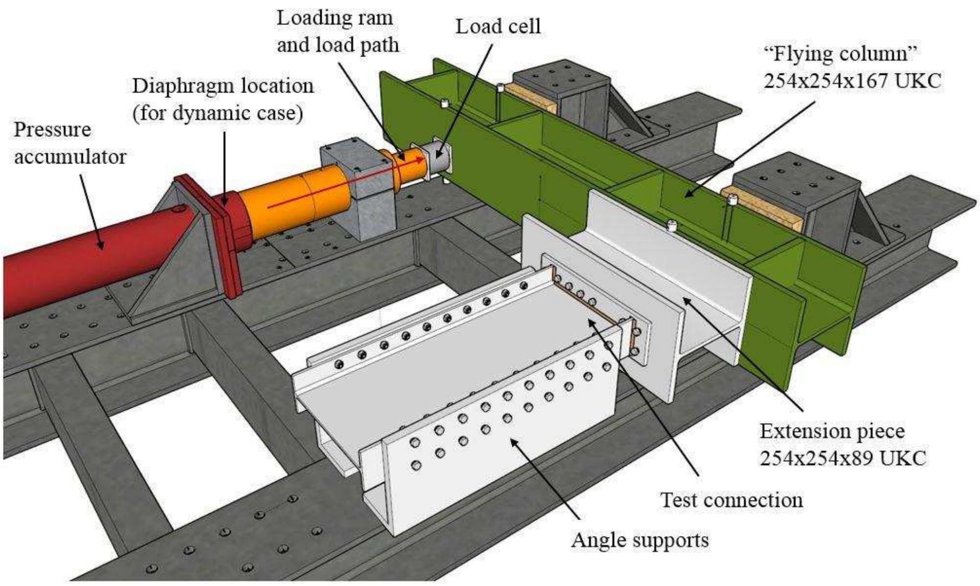

Fig. 10: 3D model of testing rig

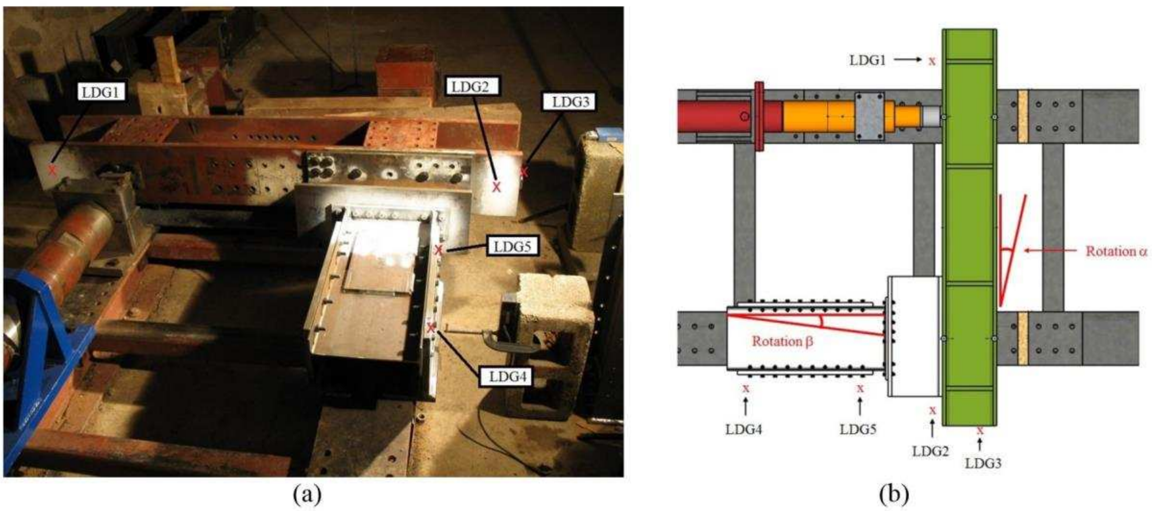

Fig. 11: Displacement measurement locations illustrated on (a) photo of rig and (b) 3D model

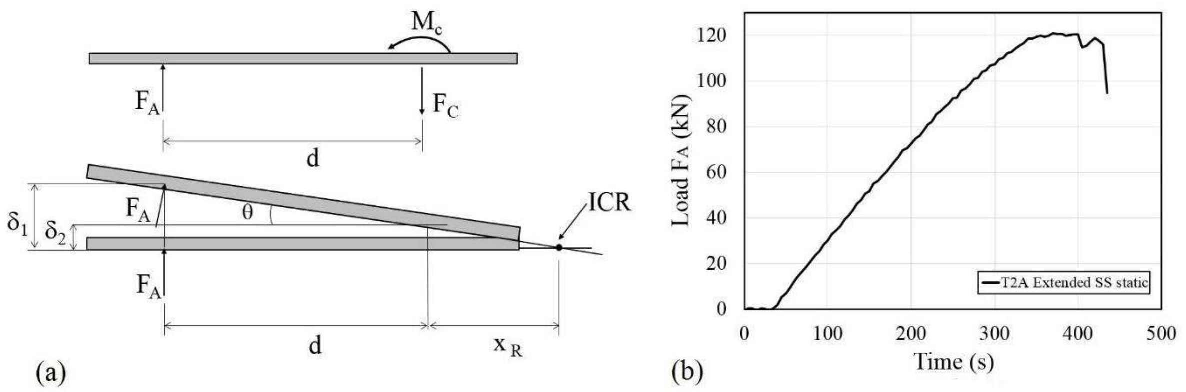

Fig. 12: Quasi-static loading scenario: (a) free body diagram and (b) test T2A load versus time

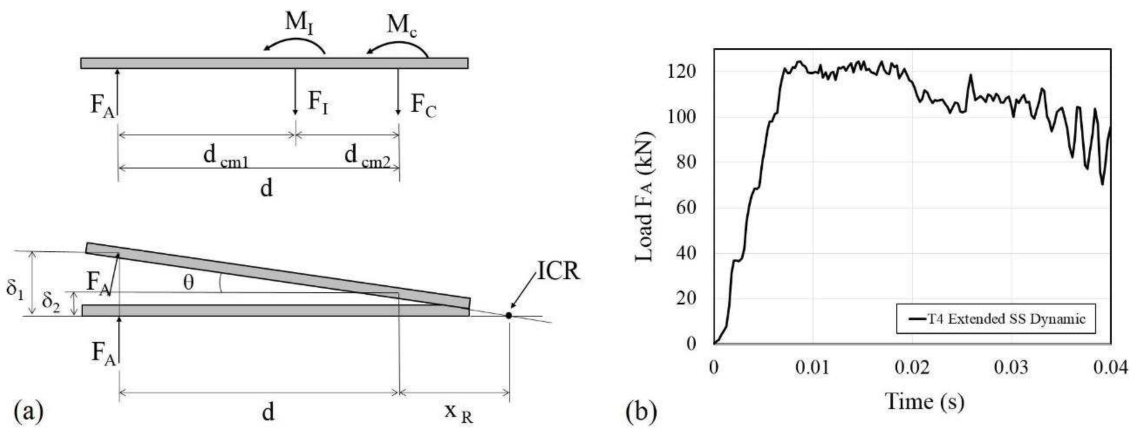

Fig. 13: Dynamic loading scenario: (a) free body diagram and (b) test T4 load versus time

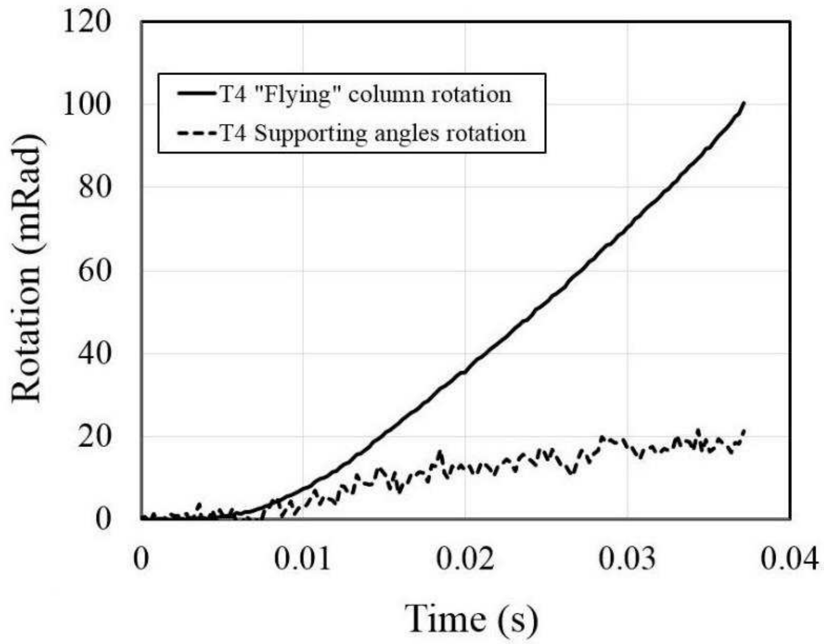

Fig. 14: Rotation versus time for dynamic test T4

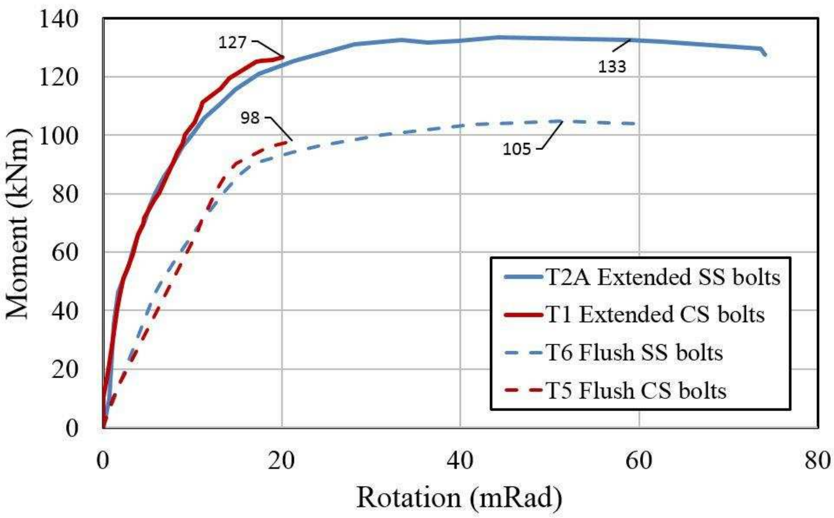

Fig. 15: Moment versus rotation for quasi-static tests

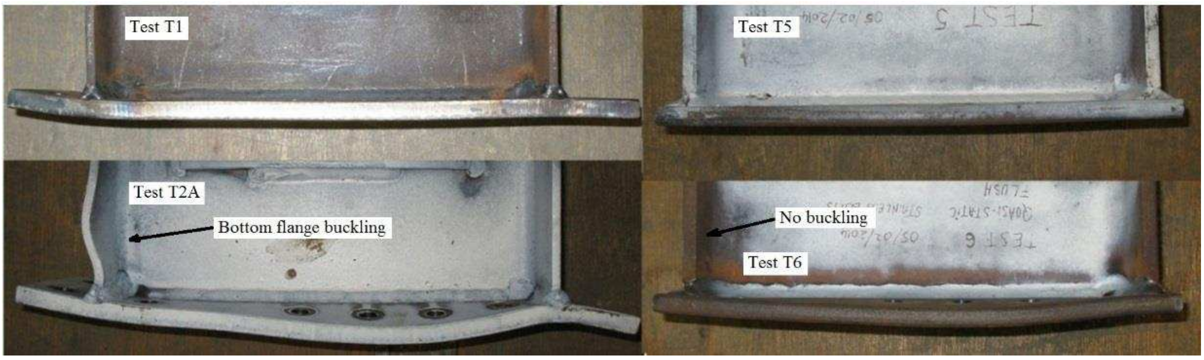

Fig. 16: Plate deformation with carbon steel (top) and stainless steel bolts (bottom) for quasi-static tests

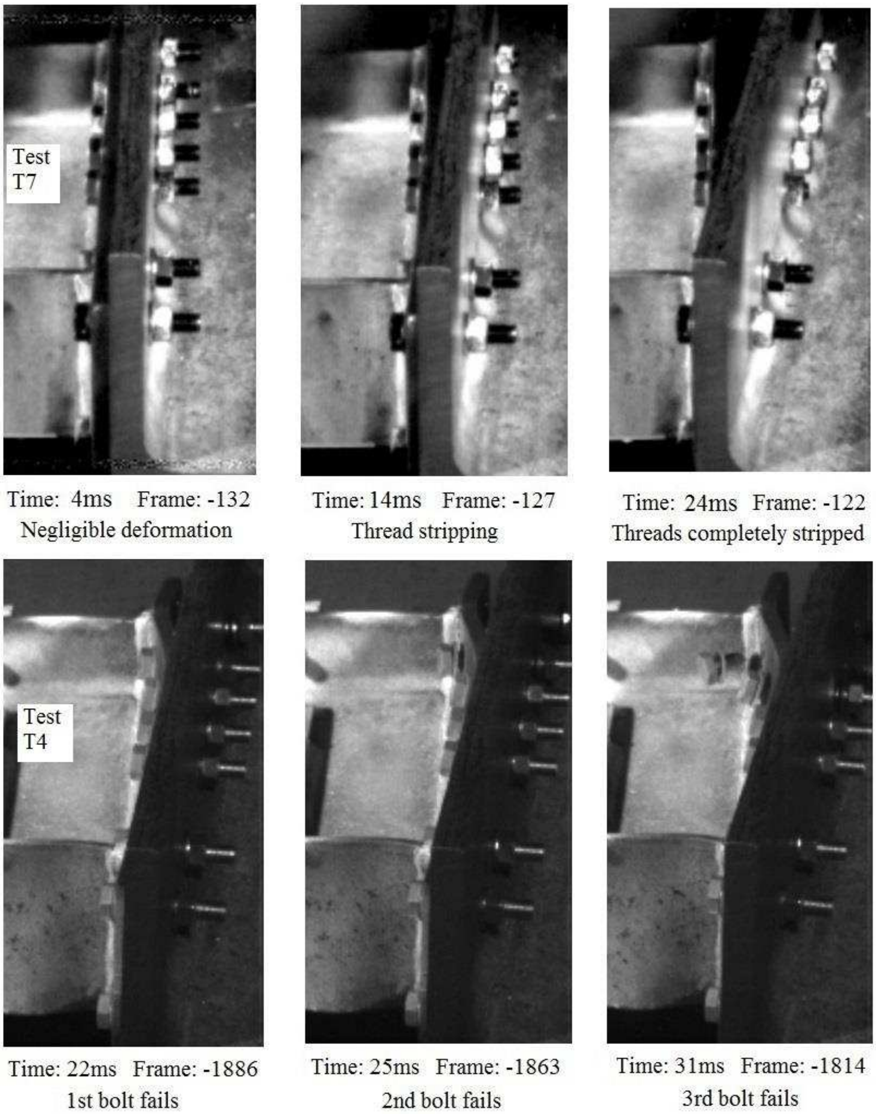

Fig. 17: Frames captured after commencement of dynamic loading for carbon steel bolted connection (top row) and stainless steel bolted connection (bottom row)

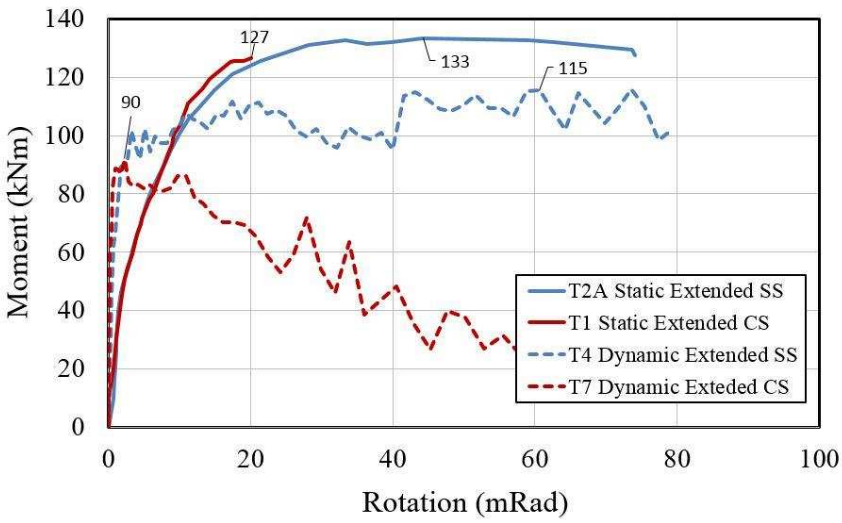

Fig. 18: Moment versus rotation for static and dynamic extended plate tests

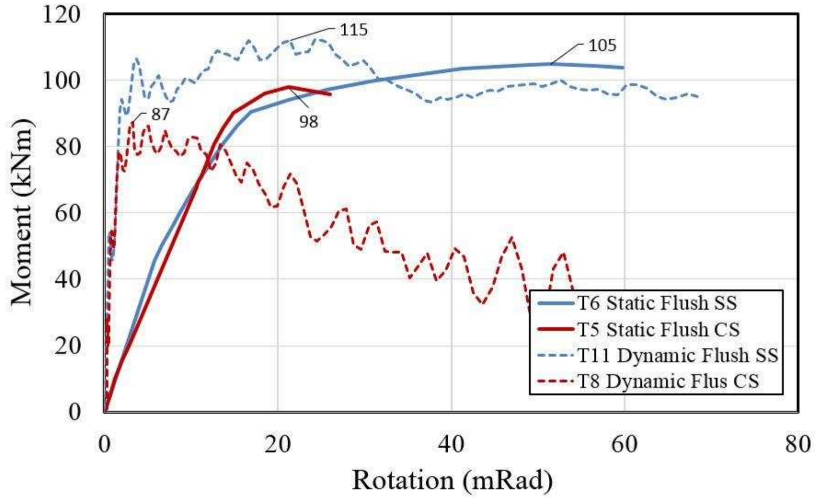

Fig. 19: Moment versus rotation for static and dynamic flush plate tests